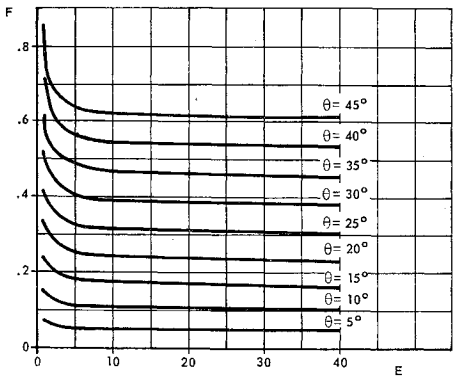

Fig. 4 Limiting view factor.

From Fig. 1 the equation for r^2 is

$$r^2 = y_1^2[(y/y_1)^2 \sec^2\theta - 2(y/y_1)\{1 + (x_1/y_1)\tan\theta\cos\phi\} + (x_1/y_1)^2 + 1] \quad (5)$$

Equation (5) is substituted into Eq. (4) and the resulting expression is integrated. The angle at the limit of sight on the conical surface is

$$\phi_0 = \cos^{-1}[(y_1/x_1)\tan\theta] \quad (6)$$

Substituting Eq. (6) for ϕ_0 and putting the solution in nondimensional form yields

$$F_{dA_1-A_2} = \frac{\sin\theta}{\pi}\tan^{-1}\left[\frac{\sec\theta}{(E^2 - \tan^2\theta)^{1/2}}(\bar{\eta} - 1)\right] + \frac{1}{\pi}\tan^{-1}\left[\frac{E + \tan\theta}{E - \tan\theta}\right]^{1/2} - \frac{(\bar{\eta} - 1)^2 + E^2 - \bar{\eta}^2\tan^2\theta}{[(\bar{\eta}\tan\theta + E)^2 + (\bar{\eta} - 1)^2]^{1/2}} \times \frac{}{[(\bar{\eta}\tan\theta - E)^2 + (\bar{\eta} - 1)^2]^{1/2}} \tan^{-1}\left\{\left[\frac{(\bar{\eta}\tan\theta + E)^2 + (\bar{\eta} - 1)^2}{(\bar{\eta}\tan\theta - E)^2 + (\bar{\eta} - 1)^2}\right]^{1/2}\left(\frac{E - \tan\theta}{E + \tan\theta}\right)^{1/2}\right\} \quad (7)$$

where $\eta = y/y_1$ and $E = x_1/y_1$. Equation (7) is the expression for the view factor from the differential area to the conical surface. The only restrictions on this equation are that $E \geq \tan\theta$ and $y > 0$.

On the conical boundary ($E = \tan\theta$), Eq. (7) reduces to

$$F_{dA_1-A_2} = \sin\theta/2 + \tfrac{1}{2} \quad (8)$$

In some applications, the limiting value of the view factor as the cone length approaches infinity is of interest. From Eq. (7)

$$\lim_{\bar{\eta}\to\infty} F_{dA_1-A_2} = \frac{\sin\theta}{2} + \frac{1}{\pi}\tan^{-1}\left[\frac{E + \tan\theta}{E - \tan\theta}\right]^{1/2} - \frac{1}{\pi}\frac{1 - \tan^2\theta}{1 + \tan^2\theta}\tan^{-1}\left[\frac{E - \tan\theta}{E + \tan\theta}\right]^{1/2} \quad (9)$$

Figure 3 shows graphs of the view factor vs the distance down the cone axis for cone half-angles of 10°, 20°, 30°, and 40°. This distance is measured from the differential area (at $Y = 0$) and nondimensionalized with respect to the cone radius at the differential-area y position. Y/R_e is a more convenient parameter than η. The relation between the two nondimensional distances is

$$Y/R_e = (\eta - 1)/\tan\theta \quad (10)$$

Figure 4 is a graph of the limiting view factor (Eq. 10) vs the differential-area position factor E for various cone half-angles. This graph shows that for $E > 10$ increasing E has little effect on the limiting view factor.

Conclusions

The analysis presents a more useable result than the Bobco and Morizumi approaches because it yields an algebraic equation for the view factor. This enables rapid calculation of view factors with the slide rule or calculation machine. All of the data presented in Figs. 3 and 4 were obtained from a digital computer program that required less than 2 min execution time.

References

[1] Morizumi, S. J., "Analytical Determination of Shape Factors from a Surface Element to an Axisymmetric Surface," *AIAA Journal*, Vol. 2, No. 11, Nov. 1964, pp. 2028–2030.

[2] Bobco, R. P., "Radiation from Conical Surfaces with Nonuniform Radiosity," *AIAA Journal*, Vol. 4, No. 3, March 1966, pp. 544–546.

[3] Sparrow, E. M. and Cess, R. D., *Radiation Heat Transfer*, Brooks/Cole, Belmont, Calif., 1966.

Dynamic Plastic Response of Finite Bars

E. R. Wood* and T. H. Liu†
Georgia Institute of Technology, Atlanta, Ga.

Introduction

THIS Note examines the dynamic response of a fixed-free, finite bar subjected to an axially applied impact load where the load is sufficiently high to result in plastic strains (Fig. 1). The material of the bar is represented by a bilinear static stress-strain diagram where the elastic and plastic moduli are denoted by E_0 and E_1, respectively. By varying the slope of the plastic region of this curve (E_1/E_0), it is possible to explore the effects of strain hardening on this problem, including the limiting case of elastic wave propagation in which E_1/E_0 is equal to one.

Analysis

In the problem considered, the time history of applied normal stress at the end $x = 0$ is given by

$$\sigma(0,t) = 0, t \leq 0 \quad (1)$$

$$\sigma(0,t) = P, t > 0 \quad (2)$$

where $P > \sigma_0$ (yield stress). In this example the applied stress was selected such that $P = 4\sigma_0$. The boundary condition at the fixed end of the bar is that the particle velocity is zero at $x = L$ for all time, or

$$v(L,t) = 0 \quad (3)$$

For one-dimensional plastic waves the rate-dependent theory of Malvern[1,2] results in the following set of quasilinear partial differential equations:

$$\partial\sigma/\partial x = \rho\partial v/\partial t \quad (4)$$

$$\partial\epsilon/\partial t = \partial v/\partial x \quad (5)$$

Presented at the AIAA Structural Dynamics and Aeroelasticity Specialist Conference, New Orleans, La., April 16–17, 1969; submitted April 28, 1969; revision received August 8, 1969. This work was supported by NASA Institutional Grant NsG-657.

* Associate Professor, School of Aerospace Engineering, School of Engineering Science and Mechanics. Associate Fellow AIAA.

† Research Assistant, School of Engineering Science and Mechanics.

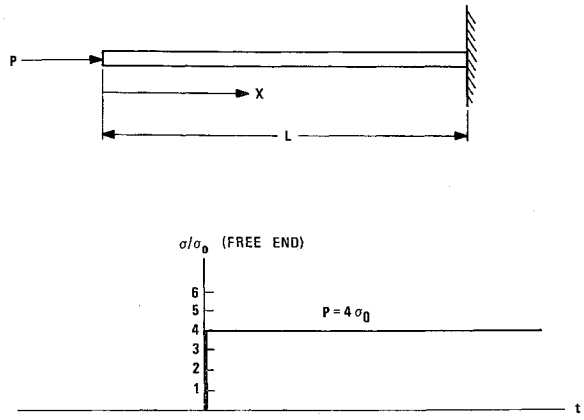

Fig. 1 The problem considered.

$$E_0\,\partial\epsilon/\partial t = \partial\sigma/\partial t + g(\sigma,\epsilon) \tag{6}$$

where σ and ϵ are the engineering stress and strain, v is the particle velocity, E_0 is Young's modulus, ρ is the initial density, t is the time, and x is the distance from the origin, where the origin represents the undisturbed position of the free end of the bar.

The recurring wave reflections that occur from each end of a finite bar result in repeated dynamic loading and unloading for each point along the bar's length. This means that a definite elastic-plastic loading-unloading criteria must be established. This question has been considered by Lubliner[3] and Cristescu[4] in relation to the Sokolovski[5]-Malvern theory given here, and for more general constitutive relations as well. As set forth by Lubliner,[3] Eq. (6) for loading and unloading may be written

$$E_0\,\partial\epsilon/\partial t = \partial\sigma/\partial t + \langle g(\sigma,\epsilon)\rangle \tag{7}$$

where

$$\langle z\rangle \equiv \begin{cases} z, & z > 0 \\ 0, & z \leq 0 \end{cases} \tag{8}$$

This simply states that during dynamic loading and unloading the elastic stress-strain relation governs whenever, at a given location, the stress falls below the static stress-strain curve $[\sigma < f(\epsilon)]$. Otherwise, the governing equation will be the rate-dependent relation given by Eq. (6). In Eq. (6) the rate-dependent term is applied in the form suggested by Malvern.[2] That is,

$$g(\sigma,\epsilon) = E_0\,\partial\epsilon''/\partial t = k[\sigma - f(\epsilon)] \tag{9}$$

where σ is the instantaneous stress, $f(\epsilon)$ is the stress at the static test, and k is a material constant that may be selected empirically to match the strain-rate characteristics of a specified material. For a bilinear stress-strain law, the function $g(\sigma,\epsilon)$ is expressed as

$$g(\sigma,\epsilon) = k[\sigma - \sigma_0(1 - E_1/E_0) - E_1\epsilon] \tag{10}$$

Equations (4–6) comprise a hyperbolic system of quasi-linear partial differential equations. These may be combined and reduced to total differentials along characteristic lines, then integrated numerically. The general method of analysis, including treatment of jump conditions across the wave front, is discussed in a related paper on semi-infinite bars by Wood and Phillips.[6]

The manner by which initial and subsequent wave reflections are included in this analysis of a finite bar is shown in Fig. 2. Once the stress is applied, it propagates toward the fixed end with the wave front moving at the elastic velocity $(E_0/\rho)^{1/2}$. This is indicated by the line OBA in the figure. At point A the first reflection occurs at the fixed end. The initiation of subsequent reflections is indicated by points N, R, W, and Z. We observe from Fig. 2 that region I

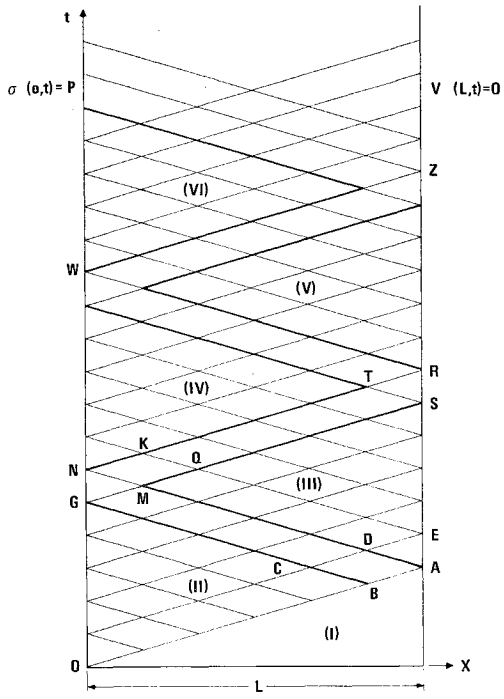

Fig. 2 Characteristics diagram showing method of analysis for wave reflections.

represents the stress-free undisturbed region, region II is the initially stressed region with no reflected waves, whereas regions III, IV, V, and all subsequent regions are those where wave reflection and interaction is occurring.

The procedure carried out in the analysis was to first perform numerical integration in region II to determine stresses, strains, and particle velocities at all points. This yielded B and C (see Fig. 2) as known values. Stresses and strains at point A could then be determined from the following conditions:

$$\text{along } dx/dt = c_0,\ d\sigma - \rho c_0 dv = -g(\sigma,\epsilon)dt \tag{11}$$

$$\text{at point } A(x = L),\ v(L,t) = 0,\ d\sigma = E_0 d\epsilon \tag{12}$$

The corresponding finite-difference equations are

$$\sigma_A - \sigma_B - \rho c_0(v_A - v_B) = -\tfrac{1}{2}(g_A + g_B)\Delta t \tag{13}$$

$$v_A = 0,\ \sigma_A = E_0\epsilon_A \tag{14}$$

where the elastic stress-strain relation at point A results from the instantaneous loading at this point due to the reflection of a sharp wave front. With A, B, and C known, D is readily obtained from the basic finite-difference equations (see Ref. 6). All points along AM can now be found. Region III has thus been linked with region II. The remaining calculations for region III are carried out in a routine manner. By a similar approach region IV can be joined to region III. Here, first N would be found, then K from M, N, and Q. This now makes it possible to find the values along the characteristic NT making use of known values along characteristic MS.

Following this procedure, each region is linked to the preceding. For the calculations, the bar was subdivided into twelve equal lengths and a time increment selected where $k\Delta t = 1$. This resulted in stress, strain, and velocity values being determined for 78 points for each triangular region shown by Fig. 2.

Numerical Results

Representative results showing the influence of strain hardening on the dynamic response are given in Fig. 3. Shown is a plot of stress as a function of x, distance along

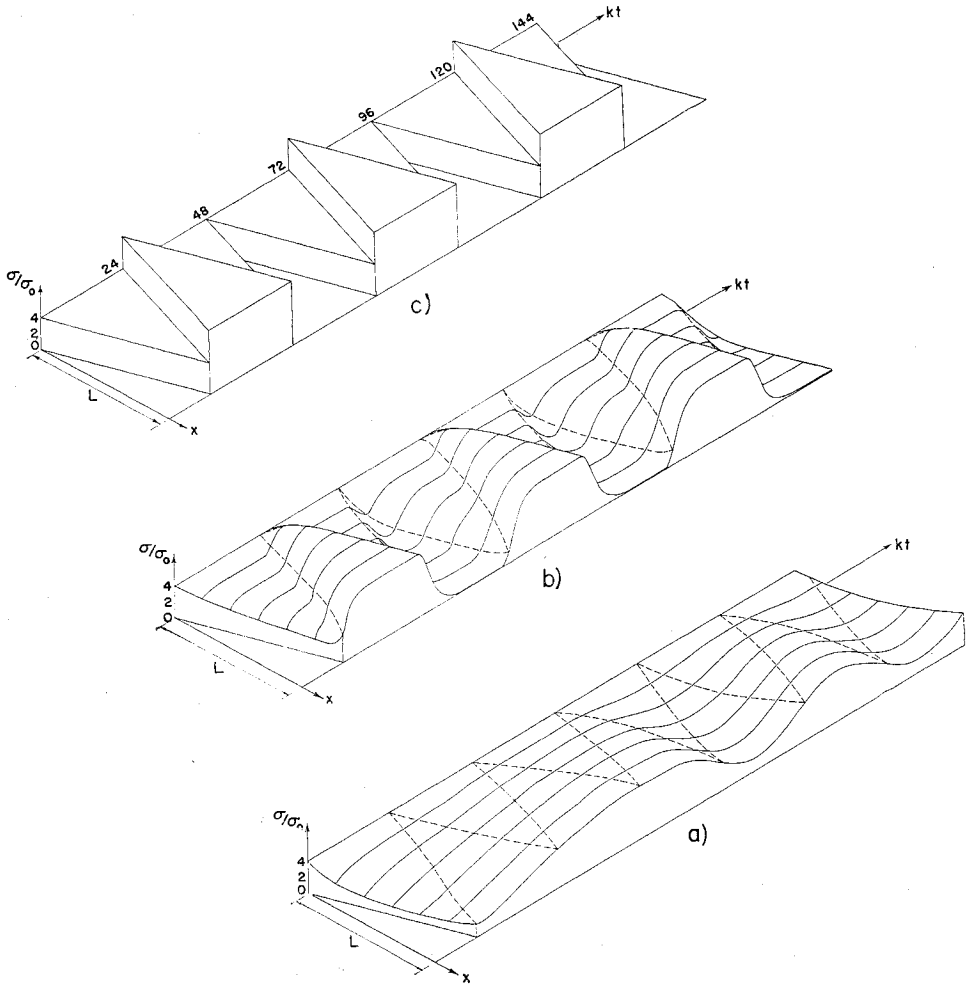

Fig. 3 Three-dimensional plots of stress in the Lagrangian x-t plane comparing the elastic and two plastic solutions.

the bar, and t, time for three cases. Figure 3a gives the dynamic response for the case when the material is very plastic, that is, $E_1/E_0 = \frac{1}{9}$. If we increase strain hardening such that the material is nearly elastic ($E_1/E_0 = \frac{7}{9}$), then we obtain the response shown in Fig. 3b. Finally, for the elastic case ($E_1/E_0 = 1$) the results are as given in Fig. 3c. The elastic solution shown by Fig. 3c can also be obtained by a normal mode solution.

Study of Fig. 3 indicates several interesting trends. As the ratio E_1/E_0 increases (an increase in strain hardening), we observe that the character of the response changes significantly. Also, if we examine the time history of stress at the fixed end of the bar ($x = L$), we note that the time required for the stress to build up to its maximum value increases as the material becomes more plastic. This is due to the contribution of the rate-dependent term [see Eq. (9)] which increases (for a given stress-strain level) as the ratio E_1/E_0 decreases. We find that in the limit when the material becomes perfectly plastic ($E_1/E_0 \rightarrow 0$), the time required for the stress at the fixed end to build up becomes infinite. In this case, the bar cannot support a stress in excess of the yield stress.

Of interest to the designer is the result that as the material becomes more plastic there is also a reduction in the maximum stress attained immediately after impact. Recalling that the applied stress is $\sigma/\sigma_0 = 4.0$, we find for the elastic case ($E_1/E_0 = 1.0$) that the fixed end stress doubles under dynamic loading to $\sigma/\sigma_0 = 8.0$ in accordance with classical theory. But, as the material becomes more plastic, there is an increasing reduction in this peak stress value, which approaches $\sigma/\sigma_0 = 4.0$ as a limit, for all but perfectly plastic materials.

The computer results plotted in Fig. 3 also indicate that after initial stress buildup, the stress at each point on the bar oscillates periodically. Oscillations occur at the fundamental frequency of the bar. (For the problem considered, $t = 48/k$ or $\omega = \pi k/24$.) Plastic deformation occurs during the initial stress buildup period, whereas subsequent oscillations are due to a residual elastic wave that travels back and forth along the bar. The oscillation occurs about a mean value $\sigma/\sigma_0 = 4.0$, which is the applied stress at the free end. Note that as the material becomes more plastic there is a reduction in the amplitude of the oscillating stress. Observe that the shape of the resulting periodic function (for a given position x of the bar) varies considerably with the degree of strain hardening. As the material becomes more plastic it is noted there is less contribution of higher modes to the response. It was found for ratios of E_1/E_0 less than $\frac{1}{2}$ that the steady-state response resulting from a step-load input was essentially first mode in character.

References

[1] Malvern, L. E., "Plastic Wave Propagation in a Bar of Material Exhibiting a Strain Rate Effect," *Quarterly of Applied Mathematics*, Vol. 8, Jan. 1951, pp. 405–411.

[2] Malvern, L. E., "The Propagation of Longitudinal Waves of Plastic Deformation in a Bar of Material Exhibiting a Strain Rate Effect," *Journal of Applied Mechanics*, Vol. 18, March 1951, pp. 203–208.

[3] Lubliner, J., "A Generalized Theory of Strain-Rate-Dependent Plastic Wave Propagation in Bars," *Journal of the Mechanics and Physics of Solids*, Vol. 12, Feb. 1964, pp. 59–65.

[4] Cristescu, N., "Loading/Unloading Criteria for Rate Sensitive Materials," *Archinum Mechaniki Stosowanej*, Vol. 17, No. 2, Feb. 1965, pp. 291–304.

[5] Sokolovski, V. V., "The Propagation of Elastic-Viscoplastic Waves in Bars," *Prikladnaya Matematika i Mekhanika*, Vol. 12, No. 3, 1948, pp. 261–280.

[6] Wood, E. R. and Phillips, A., "On the Theory of Plastic Wave Propagation in a Bar," *Journal of the Mechanics and Physics of Solids*, Vol. 15, July 1967, pp. 241–254.